

3-D migration of cross-spread data: Resolution and amplitude aspects

C. P. A. Wapenaar*

ABSTRACT

Ideally, full prestack migration involves a 4-D integration along the source and receiver coordinates. Obviously, for cross-spread data (typical for land acquisition) this 4-D integration cannot be effectuated. An analysis is presented of the resolution and amplitude behavior of full prestack migration, applied to cross-spread data. Moreover, a proposal is made to modify operators that partly compensate for the diminishing effects of the cross-spread acquisition geometry on amplitudes and resolution.

INTRODUCTION

Three-dimensional migration schemes are based on the assumption that the seismic data have been measured on a 2-D regular grid. In particular, ideal full prestack migration involves a numerical evaluation of a 4-D integral along the source coordinates (x_S, y_S) and along the receiver coordinates (x_R, y_R) . In practice, this 4-D integration can never be accomplished because of the acquisition limitations, such as in cross-spread configurations that are usually encountered in land acquisition (von Seggern, 1994; Vermeer, 1994).

The most straightforward way of dealing with incomplete data is by treating the "missing" data as empty traces. As a result, the spatial resolution decreases and the amplitudes are imaged erroneously. In principle, these problems can be partly overcome by inversion techniques based on iterative data fitting (Sevink and Herman, 1995). However, five iterations are required typically, where the cost of each iteration is comparable with twice the cost of prestack migration. Probably a more efficient approach is the computation and use of the "Beylkin determinant" (Bleistein, 1987) for the specific acquisition configuration. However, results of this approach for cross-spread data have never been published.

The aim of this paper is to analyze the effects of a typical cross-spread acquisition configuration on full prestack

migration and to propose modified operators that compensate partly for these effects. For simplicity, a homogeneous macro model (with propagation velocity c) will be assumed.

FORWARD MODEL OF 3-D DATA

Assuming a unit point source at $(x_S, y_S, z_S = 0)$ and a unit point diffractor at $(x_D, y_D, z_D > 0)$, the response measured by a unit point receiver at $(x_R, y_R, z_R = 0)$ is in the frequency domain given by the product of two propagation operators, according to

$$P(x_R, y_R, 0 | x_S, y_S, 0) = W(x_R - x_D, y_R - y_D, z_D) \times W(x_D - x_S, y_D - y_S, z_D), \quad (1)$$

(the angular frequency ω is omitted for notational convenience; throughout this paper I consider positive ω only). Various choices are possible for the operator $W(x, y, z)$, depending on the type of source, diffractor, etc. For convenience I choose dipole point-source responses, according to

$$W(x, y, z) = \frac{1}{2\pi} \frac{1 + jkr}{r} \frac{z e^{-jkr}}{r}, \quad (2)$$

for $z > 0$, with $r = \sqrt{x^2 + y^2 + z^2}$ and $k = \omega/c$. The motivation for this choice is that the double spatial Fourier transform of W is given by the well known phase-shift operator, according to

$$\int_{-\infty}^{\infty} \int_{-\infty}^{\infty} W(x, y, z) e^{j(k_x x + k_y y)} dx dy = \tilde{W}(k_x, k_y, z) = e^{-jk_z z}, \quad (3)$$

for $z > 0$, with $k_z = \sqrt{k^2 - k_x^2 - k_y^2}$. As a consequence the inverse operator F , required for downward extrapolation, is well approximated by the matched filter, according to $F(x, y, z) = W^*(-x, -y, z) = W^*(x, y, z)$, where $*$ denotes complex conjugation.

Manuscript received by the Editor December 5, 1995; revised manuscript received August 5, 1996.

*Delft University of Technology, Centre for Technical Geoscience, Laboratory of Seismics and Acoustics, Lorentzweg 1, 2628 CJ Delft, Netherlands.

E-mail: kees@akst12.tn.tudelft.nl.

© 1997 Society of Exploration Geophysicists. All rights reserved.

3-D DOWNWARD EXTRAPOLATION

Complete data

In this subsection it is assumed that the data, described in the previous section, are available on a complete 4-D (x_S, y_S, x_R, y_R) -grid. Full prestack 3-D downward extrapolation to an arbitrary depth level $z > 0$ consists of two 2-D spatial deconvolution processes along the source and receiver coordinates, according to

$$P_0(x, y, z) = \iiint F(x - x_R, y - y_R, z) \times P(x_R, y_R, \mathbf{0} | x_S, y_S, \mathbf{0}) \times F(x_S - x, y_S - y, z) dx_R dy_R dx_S dy_S, \quad (4)$$

(Berkhout, 1985). Here $P_0(x, y, z)$ is a short notation for $P(x, y, z | x, y, z)$. Imaging usually consists of an integration of $P_0(x, y, z)$ over all frequencies. This is not discussed further in this paper.

Substitution of the forward model, defined in equation (1), gives

$$P_0(x, y, z) = P_R(x, y, z) P_S(x, y, z), \quad (5)$$

where

$$P_R(x, y, z) = \iint_{-\infty}^{\infty} F(x - x_R, y - y_R, z) \times W(x_R - x_D, y_R - y_D, z_D) dx_R dy_R, \quad (6)$$

$$P_S(x, y, z) = P_R(x, y, z). \quad (7)$$

Using some basic results of Fourier theory, $P_R(x, y, z)$ may be expressed in terms of the double spatial Fourier transforms of W and F , according to

$$P_R(x, y, z) = \frac{1}{4\pi^2} \iint_{-\infty}^{\infty} \tilde{F}(k_x, k_y, z) \times \tilde{W}(k_x, k_y, z_D) e^{-j(k_x(x-x_D) + k_y(y-y_D))} dk_x dk_y, \quad (8)$$

where $\tilde{W}(k_x, k_y, z)$ is given in equation (3) and where $\tilde{F}(k_x, k_y, z) = \tilde{W}^*(k_x, k_y, z)$. Note that $\tilde{F}(k_x, k_y, z_D) \tilde{W}(k_x, k_y, z_D) = 1$ for propagating waves (i.e., for $k_x^2 + k_y^2 \leq k^2$), whereas this product is negligible for evanescent waves (i.e., for $k_x^2 + k_y^2 > k^2$), see Figure 1. Hence, ignoring evanescent waves, for $z = z_D$ equation (8) yields

$$P_R(x, y, z_D) = \frac{k}{2\pi} \frac{J_1(k\xi)}{\xi} \quad (9)$$

(Berkhout, 1984), where $\xi = \sqrt{(x - x_D)^2 + (y - y_D)^2}$ and where J_1 is the first-order Bessel function. Using equation (5) yields

$$P_0(x, y, z_D) = \frac{k^2}{4\pi^2} \frac{J_1^2(k\xi)}{\xi^2}, \quad (10)$$

see Figure 2. This result represents the (monochromatic) response of the diffractor, “measured” at the depth level of the diffractor (and therefore it is independent of z_D). However, instead of a spatial delta function, a circular symmetric resolution function is observed. Apparently the resolution is finite, despite the fact that the aperture is infinite. This is because of the suppression of the evanescent wavefield by the matched filter.

[For a further discussion on this “infinite aperture paradox,” see Wapenaar (1992)]. The width of the main lobe (measured at the first “zero crossing”) is approximately $6\lambda/5$, where λ is the wavelength, defined as $\lambda = 2\pi/k$. Note that the side lobes have very low amplitudes.

Next, consider an infinite horizontal perfect reflector at depth z_D . This reflector may be seen as a continuous distribution of diffractors at depth level z_D , hence, the downward extrapolation result is obtained by integrating the right-hand side of equation (10) along x_D and y_D , according to

$$\iint_{-\infty}^{\infty} \iint_{-\infty}^{\infty} \frac{k^2}{4\pi^2} \frac{J_1^2(k\xi)}{\xi^2} dx_D dy_D = \frac{k^2}{4\pi^2} \int_0^{\infty} \frac{J_1^2(k\xi)}{\xi^2} \xi d\xi \int_0^{2\pi} d\theta = \frac{k^2}{4\pi}, \quad (11)$$

[Abramowitz and Stegun, 1970, equation (11.4.6)]. This result represents the (monochromatic) spatially band-limited response of the reflector, “measured” at the reflector. The

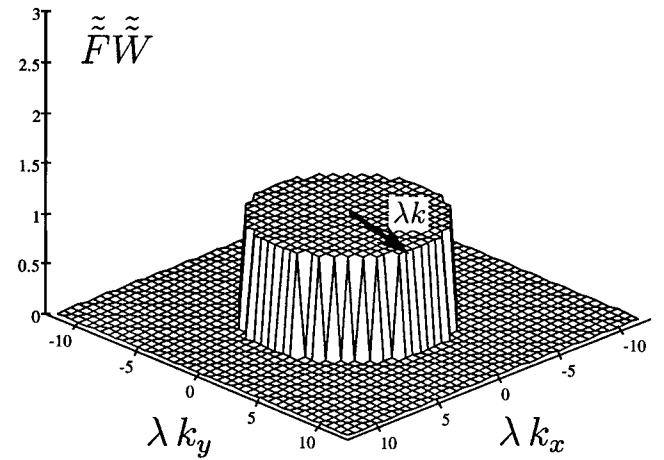


FIG. 1. The matched filter perfectly inverts propagating waves (the area within the circle), whereas it suppresses evanescent waves. (The axes have been scaled by the wavelength λ . Hence, the scaled radius of the area covered by the propagating wave field equals $\lambda k = 2\pi$).

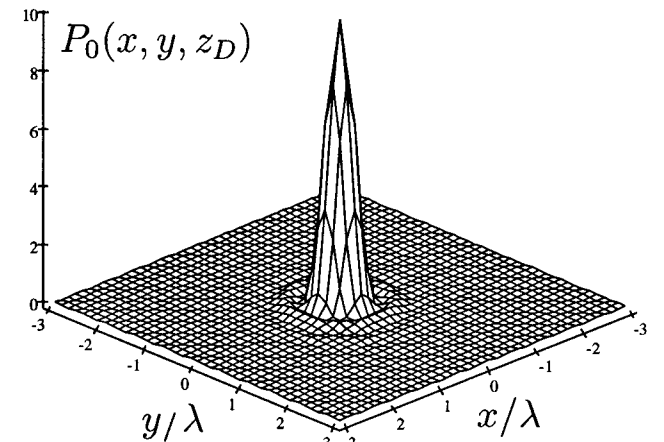


FIG. 2. Resolution function for complete acquisition. The situation is shown for $x_D = y_D = 0$.

amplitude is proportional to k^2 , which corresponds to the spatial bandwidth, see Figure 1. Note that for true-amplitude imaging, a correction factor of $4\pi/k^2$ should be applied prior to the integration along the frequency axis.

Cross-spread data

In this subsection 3-D downward extrapolation is analyzed for the incomplete data acquisition configuration shown in Figure 3. This configuration, which contains sources only along the x -axis and receivers only along the y -axis, may be seen as the “basic cross-spread configuration” for land acquisition. Making the substitution

$$P(x_R, y_R, \mathbf{0} \mid x_S, y_S, \mathbf{0}) \rightarrow \delta(x_R) P(x_R, y_R, \mathbf{0} \mid x_S, y_S, \mathbf{0}) \delta(y_S) \quad (12)$$

in equation (4) for 3-D downward extrapolation yields

$$P_0(x, y, z) = \int_{-\infty}^{\infty} \int_{-\infty}^{\infty} F(x, y - y_R, z) P(\mathbf{0}, y_R, \mathbf{0} \mid x_S, \mathbf{0}, \mathbf{0}) \times F(x_S - x, -y, z) dy_R dx_S. \quad (13)$$

Again, taking $P(\mathbf{0}, y_R, \mathbf{0} \mid x_S, \mathbf{0}, \mathbf{0})$ the response of a diffractor at (x_D, y_D, z_D) , according to the equation (1), yields

$$P_0(x, y, z) = P_R(x, y, z) P_S(x, y, z), \quad (14)$$

where

$$P_R(x, y, z) = \int_{-\infty}^{\infty} F(x, y - y_R, z) \times W(-x_D, y_R - y_D, z_D) dy_R \quad (15)$$

and

$$P_S(x, y, z) = \int_{-\infty}^{\infty} W(x_D - x_S, y_D, z_D) \times F(x_S - x, -y, z) dx_S. \quad (16)$$

Note that this time P_R and P_S are different. In a similar way as before, $P_R(x, y, z)$ may be expressed in terms of the *single* spatial Fourier transforms of W and F , according to

$$P_R(x, y, z) = \frac{1}{2\pi} \int_{-\infty}^{\infty} \tilde{F}(x, k_y, z) \times \tilde{W}(-x_D, k_y, z_D) e^{-jk_y(y-y_D)} dk_y, \quad (17)$$

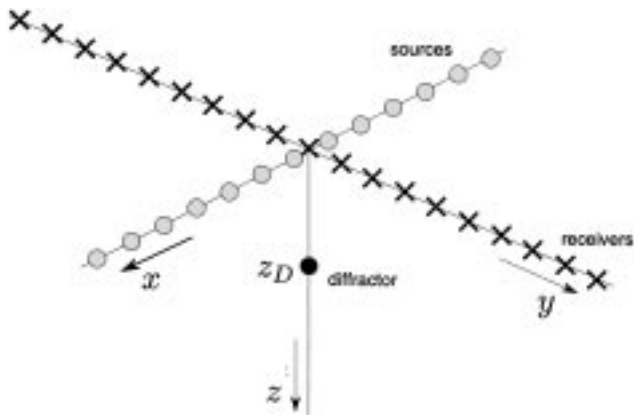


FIG. 3. Basic configuration for cross-spread acquisition. The situation is shown for $x_D = y_D = 0$.

where

$$\tilde{W}(x, k_y, z) = \int_{-\infty}^{\infty} W(x, y, z) e^{jk_y y} dy, \quad (18)$$

with $W(x, y, z)$ given by equation (2), and

$$\tilde{F}(x, k_y, z) = \tilde{W}^*(x, k_y, z). \quad (19)$$

We evaluate the integral in equation (18) using the method of stationary phase (Bleistein, 1984). Upon substitution of the high-frequency approximation of $W(x, y, z)$, equation (18) can be written as

$$\tilde{W}(x, k_y, z) \approx \int_{-\infty}^{\infty} f(y) e^{jk\phi(y)} dy, \quad (20)$$

where

$$\phi(y) = -\sqrt{y^2 + \zeta^2} + k_y y/k, \quad (21)$$

$$f(y) = \frac{jkz}{2\pi(y^2 + \zeta^2)}, \quad (22)$$

with $\zeta = \sqrt{x^2 + z^2}$. Solving $\phi'(y_0) = 0$ yields the following expression for the stationary point

$$y_0 = k_y \zeta / \kappa_z, \quad (23)$$

with $\kappa_z = \sqrt{k^2 - k_y^2}$. For $k\zeta \gg 1$ the stationary phase approximation of equation (18) thus becomes

$$\begin{aligned} \tilde{W}(x, k_y, z) &\approx \sqrt{\frac{2\pi}{|k\phi''(y_0)|}} f(y_0) e^{j(k\phi(y_0) - \pi/4)} \\ &= \sqrt{\frac{j\kappa_z}{2\pi}} \frac{z}{\zeta^{3/2}} e^{-jk_z \zeta}. \end{aligned} \quad (24)$$

Substituting this result in equation (17) and evaluating the integral for propagating waves only, yields

$$P_R(x, y, z) \approx \frac{zz_D}{2\pi(\zeta \zeta_D)^{3/2}} \times \int_{-k}^k \frac{\kappa_z}{2\pi} e^{-jk_z(\zeta_D - \zeta)} e^{-jk_y(y-y_D)} dk_y, \quad (25)$$

with $\zeta_D = \sqrt{x_D^2 + z_D^2}$. Assuming $|x^2 - x_D^2| \ll z_D^2$, for $z = z_D$ one obtains

$$P_R(x, y, z_D) \approx \frac{z_D^2}{4\pi^2 \zeta_D^3} \int_{-k}^k \kappa_z e^{-jk_y(y-y_D)} dk_y. \quad (26)$$

Using the coordinate transformation $k_y = k \cos \theta$ yields

$$P_R(x, y, z_D) \approx \frac{k^2 z_D^2}{4\pi^2 \zeta_D^3} \int_0^\pi \sin^2 \theta e^{-jk(y-y_D) \cos \theta} d\theta. \quad (27)$$

Substituting $\sin^2 \theta = \frac{1}{2} - \frac{1}{2} \cos 2\theta$ and using Abramowitz and Stegun (1970, equations 9.1.21 and 9.1.27) we obtain (see Figure 4)

$$P_R(x, y, z_D) \approx \frac{kz_D^2}{2\pi(x_D^2 + z_D^2)^{3/2}} \frac{J_1(k(y-y_D))}{2(y-y_D)}. \quad (28)$$

For fixed (x_D, y_D, z_D) , this function may be seen as the resolution function of the receiver array.

In a similar way, equation (16) yields for $|y^2 - y_D^2| \ll z_D^2$ (see Figure 5)

$$P_S(x, y, z_D) \approx \frac{kz_D^2}{2\pi(y_D^2 + z_D^2)^{3/2}} \frac{J_1(k(x - x_D))}{2(x - x_D)}. \quad (29)$$

For fixed (x_D, y_D, z_D) , this function may be seen as the resolution function of the source array.

Using equation (14) one finally obtains (see Figure 6)

$$P_0(x, y, z_D) \approx \frac{k^2 z_D^4}{4\pi^2(x_D^2 + z_D^2)^{3/2}(y_D^2 + z_D^2)^{3/2}} \times \frac{J_1(k(x - x_D))J_1(k(y - y_D))}{4(x - x_D)(y - y_D)}. \quad (30)$$

For fixed (x_D, y_D, z_D) , this function may be seen as the resolution function of the cross-spread acquisition configuration of Figure 3. The width of the main lobe, measured along the diagonal, is $\sqrt{2}$ times the width of the main lobe in Figure 2. Also the side lobes are more pronounced than in Figure 2. However, taking the severe incompleteness of the data into

account (Figure 3), it may be concluded that the resolution is quite acceptable. A more serious problem is given by the fact that the peak value of $P_0(x, y, z_D)$ in equation (30) depends on the diffractor position, according to (see Figure 7)

$$\max(P_0(x, y, z_D)) = \frac{k^4 z_D^4}{64\pi^2(x_D^2 + z_D^2)^{3/2}(y_D^2 + z_D^2)^{3/2}}. \quad (31)$$

This implies that a reflector with constant amplitude at $z = z_D$ will be imaged with a varying amplitude. This is confirmed by the following numerical experiment. Figure 8 shows a rectangular reflector centered below the acquisition configuration. The depth is chosen to be $z_D = 10\lambda$, with $\lambda = 30$ m. The response of this reflector was modeled with equation (1) for a grid of 17×17 diffractors, equally distributed along the reflector, with a grid spacing of 12 m in both directions. Downward extrapolation to $z = z_D$ was carried out by numerically evaluating the integrals in equation (13). The result, which is shown in Figure 9, indeed exhibits a similar amplitude distribution as Figure 7. In the next section, a true-amplitude operator will be proposed that compensates for the erroneous amplitude distribution observed in Figures 7 and 9.

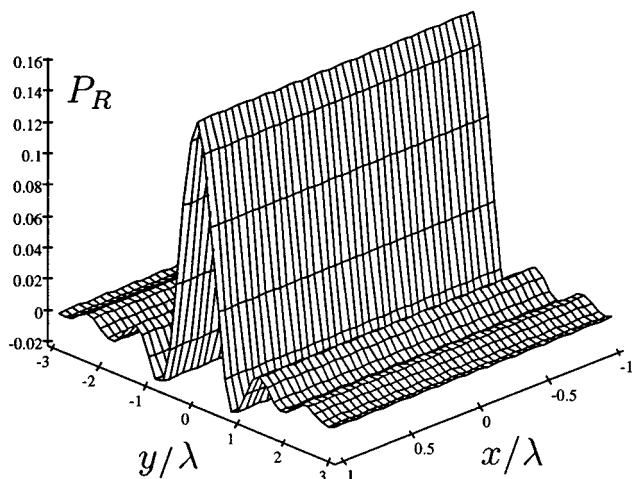


FIG. 4. Resolution function of the receiver array. The situation is shown for $x_D = y_D = 0$ and $z_D = 10\lambda$.

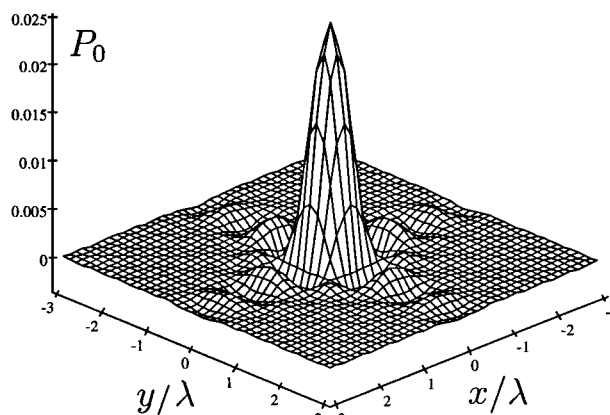


FIG. 6. Resolution function of the cross-spread acquisition configuration. The situation is shown for $x_D = y_D = 0$ and $z_D = 10\lambda$.

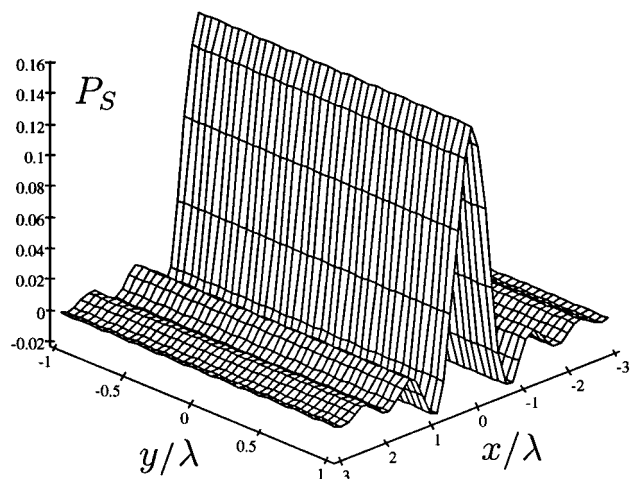


FIG. 5. Resolution function of the source array. The situation is shown for $x_D = y_D = 0$ and $z_D = 10\lambda$.

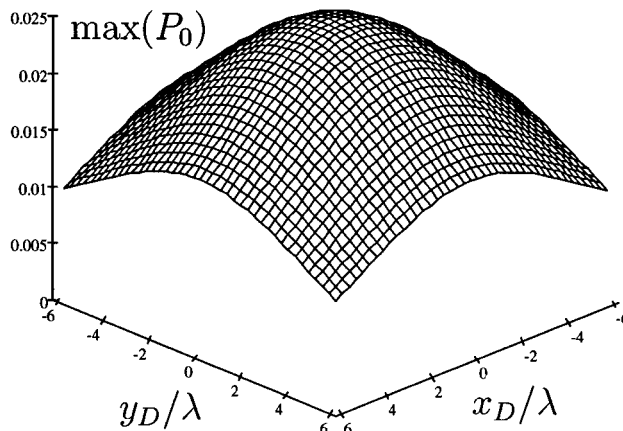


FIG. 7. Peak value of the resolution function for variable diffractor coordinates x_D, y_D at $z_D = 10\lambda$.

DESIGN OF TRUE-AMPLITUDE OPERATORS

For the compensation of the amplitude factor in equation (28), several options are available. Here the most straightforward approach is followed, i.e., the matched filter $F(x, y, z) = W^*(x, y, z)$ in equation (15) is replaced by

$$F_R(x, y, z) = \frac{2\pi(x^2 + z^2)^{3/2}}{kz^2} W^*(x, y, z), \quad (32)$$

with $W(x, y, z)$ defined in equation (2). Using a similar analysis as in the previous section one obtains instead of equation (28)

$$P_R(x, y, z_D) \approx \frac{J_1(k(y - y_D))}{2(y - y_D)}. \quad (33)$$

Similarly, by replacing the matched filter in equation (16) by

$$F_S(x, y, z) = \frac{2\pi(y^2 + z^2)^{3/2}}{kz^2} W^*(x, y, z), \quad (34)$$

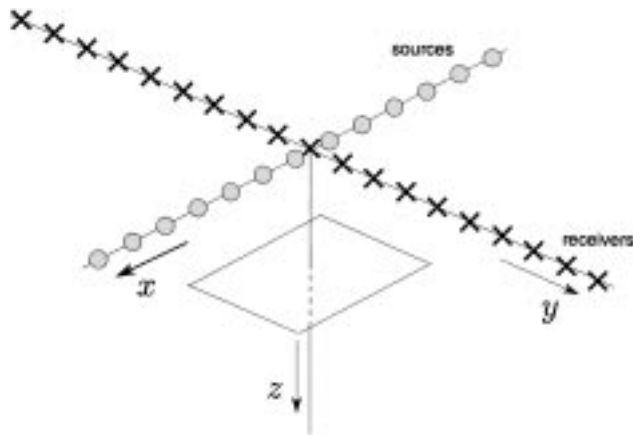


FIG. 8. Configuration for the numerical experiments. The size of the reflector is 200×200 m; its depth is 300 m.

one obtains

$$P_S(x, y, z_D) \approx \frac{J_1(k(x - x_D))}{2(x - x_D)}, \quad (35)$$

and, consequently,

$$P_0(x, y, z_D) \approx \frac{J_1(k(x - x_D))J_1(k(y - y_D))}{4(x - x_D)(y - y_D)}. \quad (36)$$

For $x_D = y_D = 0$ the resolution functions P_R , P_S , and P_0 are the same as those shown in Figure 4, 5, and 6, respectively (apart from a scaling factor). The main difference with the results in the previous section is that the peak value of $P_0(x, y, z_D)$ in equation (36) does not depend on the diffractor position. Moreover, note that

$$\int_{-\infty}^{\infty} \int_{-\infty}^{\infty} \frac{J_1(k(x - x_D))J_1(k(y - y_D))}{4(x - x_D)(y - y_D)} dx_D dy_D = 1, \quad (37)$$

(Abramowitz and Stegun, 1970, equations 11.4.16, 6.1.8, and 6.1.9), which means that a horizontal reflector will be imaged with the correct amplitude.

The experiment of the previous section was repeated, with the matched filter F replaced by F_R and F_S , as defined in equations (32) and (34), respectively. The result, which is shown in Figure 10 exhibits a constant amplitude along the reflector. Moreover, unlike in Figure 9, the value of this amplitude equals one. This confirms the true-amplitude behavior of the modified matched filters F_R and F_S .

EXTENSION TO MORE REALISTIC ACQUISITION CONFIGURATIONS

The configuration of Figure 3 represents an extreme example of spatial undersampling. A more realistic configuration is shown in Figure 11. The resolution function for this configuration is given by a superposition of shifted resolution functions related to the configuration of Figure 3. Since the amplitude and shape of these resolution functions are shift-invariant [see equation (36)], we may conclude that the resolution function for the configuration of Figure 11 is approximately given by the resolution function for the configuration of Figure 3, multiplied

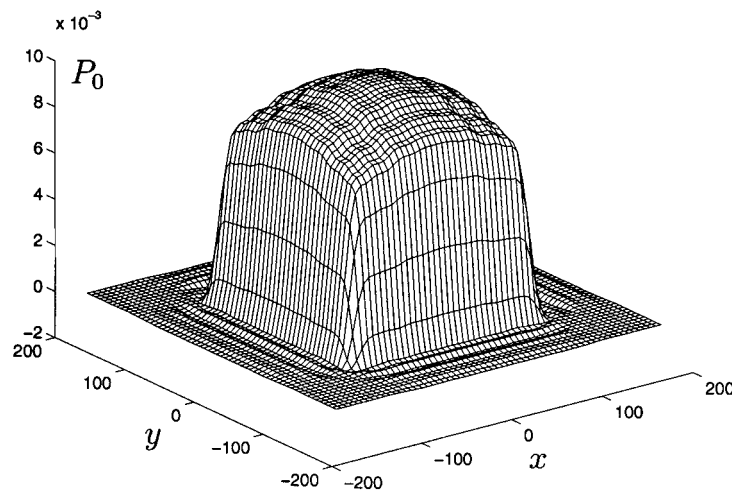


FIG. 9. Amplitude cross-section at $z = z_D$; matched filter approach (unlike in Figure 7, the horizontal axes have not been scaled by the wavelength).

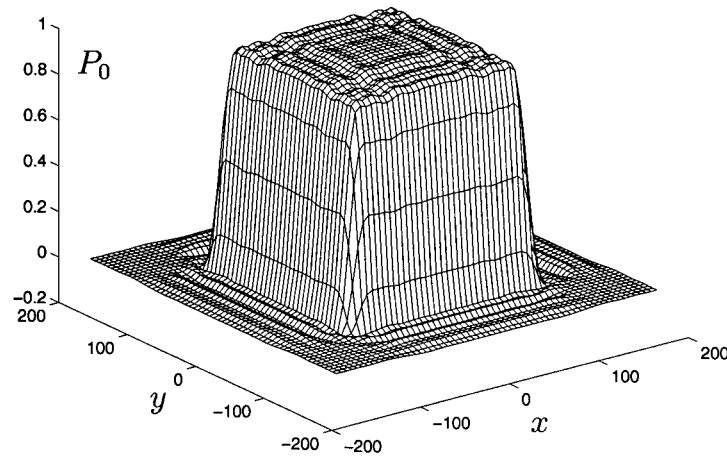


FIG. 10. Amplitude cross section at $z = z_D$: modified matched filters F_R and F_S .

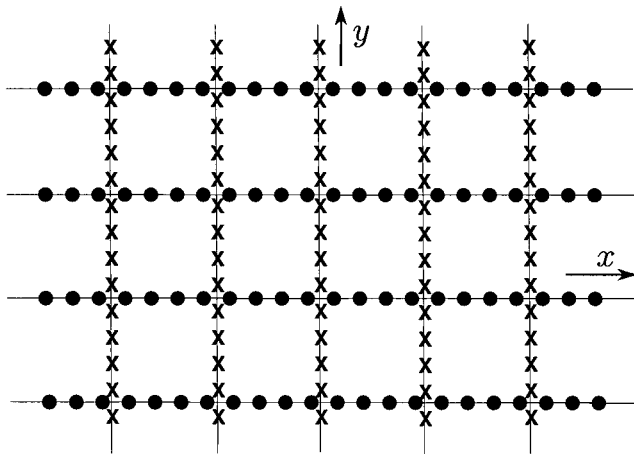


FIG. 11. Realistic 3-D land acquisition configuration: sources are properly sampled along the x -axis and severely undersampled along the y -axis; receivers are properly sampled along the y -axis and severely undersampled along the x -axis.

by the number of source lines and by the number of receiver lines. Therefore, for the acquisition configuration of Figure 11 one can apply the true-amplitude operators, given by equations (32) and (34), divided by the product of the number of source- and receiver lines that contribute to the imaging region of interest.

CONCLUSIONS

Because of the “incompleteness” of cross-spread seismic data, the spatial resolution of full prestack migration obtainable is less than what could be obtained with a complete

areal acquisition. Moreover, because the “missing data” are treated as empty traces, the imaged amplitudes are erroneous. It has been shown, for one specific acquisition configuration and a homogeneous macro model, that the downward extrapolation operators can be modified to compensate for these amplitude errors. The modified operators F_R and F_S [equations (32) and (34)] have been formulated such that they can also be applied for inhomogeneous macro models [simply by inserting for $W^*(x, y, z)$ the appropriate operator]. Of course, this will only give accurate results for moderately inhomogeneous models. The generalization for more complex media requires geometrical spreading corrections, e.g., as derived by Tygel et al. (1992).

REFERENCES

- Abramowitz, M., and Stegun, I. A., 1970, Handbook of mathematical functions: Dover Publications, Inc.
- Berkhout, A. J., 1984, Seismic resolution. A quantitative analysis of resolving power of acoustical echo techniques: Geophys. Press.
- 1985, Imaging of acoustic energy by wavefield extrapolation (3rd edition): Elsevier.
- Bleistein, N., 1984, Mathematical methods for wave phenomena: Academic Press, Inc.
- 1987, On the imaging of reflectors in the earth: Geophysics, **52**, 931-942.
- Sevink, G. J., and Herman, G. C., 1995, 3-D nonlinear asymptotic seismic inversion: Application to real and synthetic data: 65th Ann. Internat. Mtg., Soc. Expl. Geophys., Expanded Abstracts, 639-642.
- Tygel, M., Scheicher, J., and Hubral, P., 1992, Geometrical spreading corrections of offset reflections in a laterally inhomogeneous earth: Geophysics, **57**, 1054-1063.
- Vermeer, G. J. O., 1994, 3-D symmetric sampling: 64th Ann. Internat. Mtg., Soc. Expl. Geophys., Expanded Abstracts, 906-909.
- von Seggern, D., 1994, Depth-imaging resolution of 3-D seismic recording patterns: Geophysics, **59**, 564-576.
- Wapenaar, C. P. A., 1992, The infinite aperture paradox: J. Seis. Expl., **1**, 325-336.